Multiscale out-of-equilibrium dynamics driven by pulsed laser excitation in spin-crossover materials: A combined thermoelastic and mechanoelastic study

Laurentiu Stoleriu,[1] Masamichi Nishino,[2] Seiji Miyashita,[3,4,5] Alexandru Stancu,[1] Roman Bertoni,[4,6] Eric Collet,[4,6] Maciej Lorenc,[4,6] and Cristian Enachescu[1,*]

[1]*Faculty of Physics, Alexandru Ioan Cuza University of Iasi, 700506 Romania*

[2]*Research Center for Materials Nanoarchitectonics, National Institute for Materials Science, 1-1 Namiki, Tsukuba, Ibaraki 305-0044, Japan*

[3]*Department of Physics, Graduate School of Science, The University of Tokyo, 7-3-1 Hongo, Tokyo 113-0033, Japan*

[4]*DYNACOM IRL2015 University of Tokyo - CNRS - UR1, Department of Chemistry, 7-3-1 Hongo, Tokyo 113-0033, Japan*

[5]*The Physical Society of Japan, 2-31-22 Yushima, Tokyo 113-0033, Japan*

[6]*Univ Rennes, CNRS, IPR (Institut de Physique de Rennes)- UMR 6251, F-35000 Rennes, France*

(Received 20 November 2022; revised 18 May 2023; accepted 6 July 2023; published 21 July 2023)

In this paper, we present an elastic model coupled with a heat propagation process in order to reproduce the out-of-equilibrium dynamics of spin crossover materials driven by femtosecond laser excitation: a multiscale out-of-equilibrium dynamics driven by pulsed laser excitation in spin-crossover materials (thermoelastic step), the thermal switching (thermal step), and the subsequent relaxation to the initial state on cooling. The simulations were performed for open boundaries two and three-dimensional samples, composed of individual molecules linked by springs, which stand for elastic interactions. This building-up of the samples allows the propagation of elastic waves, which leads to accumulation of high spin molecules towards edges at the maximum of the thermoelastic step. We first show that a simple model with a single "temperature" reproduces the thermoelastic, the thermal step and the relaxation to the original equilibrium state. However, the too slow thermalization of the lattice obtained in this model does not correspond to the experimental data. Therefore, to overcome this drawback, we consider either an inhomogeneous photoexcitation or different "temperatures" for the lattice and the spin states. The effect of the sample size, which prevents the existence of a thermal step in the case of nanoparticles is also discussed, as well as the three-dimensional model.

DOI: 10.1103/PhysRevB.108.014306

I. INTRODUCTION

Spin crossover systems are metal complexes showing the unique ability to have two metastable spin states, high spin (HS) and low spin (LS), characterized by specific optical and magnetic properties, that can be triggered by using external stimuli, such as temperature, pressure, light [1]. The smaller cohesion energy in the HS state determines longer coordination bond lengths and larger molecular volume. A first consequence of the change of molecular volume is the existence of elastic interactions between the metal ions, which if strong enough, leads to cooperative switching accompanied by a first order phase transition (hysteresis) with temperature, light or pressure as input parameters. This property is important for practical applications, as the information storage. The thermal conversion from LS to HS state occurs at the critical temperature T_C. The LS state, stable at low temperatures, can be switched towards the long-lifetime metastable HS state by optical excitation of some specific charge transfer or metal-centred bands [2,3], with a light irradiation, by the way of the so called light induced excited spin state trapping (LIESST) effect [4,5]. Pulsed laser irradiation allows the control of this bistability in an ultrafast way, by inducing out-of-equilibrium conditions [6–12]. In solids, the initial femtosecond photoswitching is localized at molecular level, for few absorbing molecules rapidly converted towards HS state and triggers a subsequent increase of the fraction of HS molecules at longer time, driven by lattice expansion. This phenomenon is known as thermoelastic step. Recent development of elastic models for spin-crossover materials, which treat the molecular volume variation accompanied by the spin state change and elastic interactions between molecules, has clarified important cooperative properties in spin crossover phenomena [13–20]. It was demonstrated that this cooperative switching occurs due to the propagation of elastic waves, taking place on the acoustic time scale, which corresponds to the ratio between relevant spatial scale and the sound velocity in the medium [8]. The amplitude of the phenomenon is measured through the HS fraction, which is the proportion of molecules in the HS state, denoted here by X_{HS}. Yet more spectacular, the elastic step can be followed, for appropriate photoexcitation rates and system sizes, by the so-called thermal step, which is a further increase of X_{HS}, at a larger timescale due to the propagation of heat deposited by laser excitation throughout the lattice [21].

In order to understand this complex out of equilibrium behavior, where different degrees of freedom equilibrate over different spatial and time scales, we should first clarify the role

*cristian.enachescu@uaic.ro

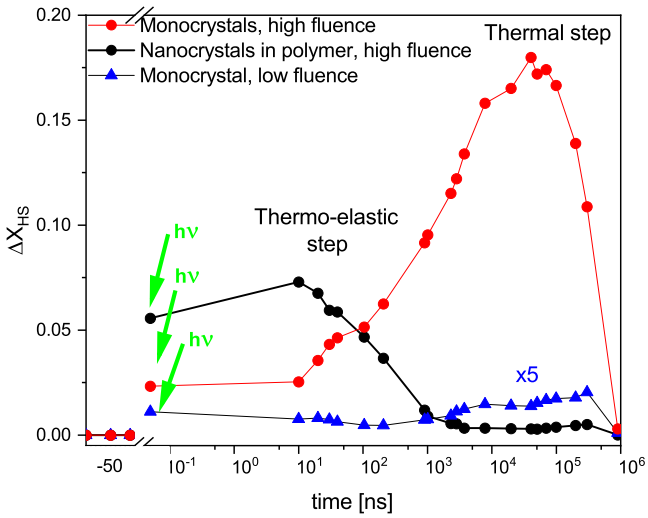

FIG. 1. Photoconversion to femtosecond laser excitation of LS $[Fe^{III}(3\text{-MeO-SalEen})]PF_6$ in the form of micro- and nanocrystals. "*hν*" denotes the photoinduced step, followed by thermoelastic and thermal steps.

of independent propagations of elastic waves and heat on the macroscopic spin state switching and what actually represents the notion of temperature. The aim of this paper is to propose a realistic model able to reproduce both elastically-driven and thermally-driven processes, considering the propagation of the elastic interactions producing the local stresses at individual molecules. The paper is organized as follows: first we present relevant experimental data, then we discuss the model, including the concept of different temperatures for the lattice and for the spin state and the simulation of the heat propagation. The main part of the paper is devoted to macroscopic and microscopic data for 2D and 3D samples, showing the effect of various parameters of the system.

II. RESULTS

A. Review on experimental data and theoretical concepts

Typical experiments showing the nonlinear response of a spin crossover system to a femtosecond laser excitation are shown in Fig. 1 for $[Fe^{III}(3\text{-MeO-SalEen})]PF_6$ samples of different sizes, which was reported in detail in Ref. [7]. The fraction of molecules switched by light from LS to HS states, within less than 1 picosecond, depends linearly on the photon excitation density, as one absorbed photon switches one molecule [22]. For higher photoexcitation density (black circles – nanocrystals in polymer, red circles – hundreds of micrometer single crystal; in Fig. 1), a self-amplified transformation towards HS state occurs within 10 ns, which is known as thermoelastic step. In addition to this first amplification, a second amplification is observed after a microseconds time in the case of single crystals (red and blue circles). In the case of nano-crystals (black circles), after the initial self-amplification, the samples relax back to the low temperature equilibrium state and no thermal step is observed. No thermal step was observed in the case of low photoexcitation (blue triangles). When the fraction of photoswitched molecules from LS to HS state is below a threshold, the LS ground state is recovered within 1 μs; in some cases a thermal step can be noticed, even in the absence of a thermoelastic step.

The increase of the high spin fraction subsequent to photoexcitation takes place in two steps, as we explain below. During ultrafast laser irradiation, a large amount of energy is locally deposited in every molecule photoexcited from LS to HS state, which causes both the local switching of electronic state and the molecular structural reorganization, together with the coherent and incoherent activation of molecular vibrational modes [23–25]. The LS-HS switching is accompanied by the increase of the molecular volume (metal-ligand distance) within less than 1 ps, which first determines the building-up and then the propagation of elastic interactions between spin crossover molecules within the crystalline lattice. This finally leads to the global lattice expansion mediated by elastic waves, which produces negative lattice pressures on individual molecules, favoring the HS state of higher volume and resulting in a fast switching of more molecules towards HS state through a cooperative elastic process [26]. After this thermoelastic expansion (thermoelastic step), HS fraction decreases for a while. On the other hand, the energy deposited into photoexcited molecules (2 eV), which far exceeds the amount needed for the LS-HS conversion (20 meV), is transferred to the surrounding lattice through vibrational cooling [27]. The distance between "hot spots (photoexcited sites)" is small for homogeneous excitation: namely, for 4% excitation one molecule over 25 absorb energy, which corresponds to one hot spot in a box of $3 \times 3 \times 3$ molecules. Therefore the energy redistribution leads to a rapid homogenization (on the order of a dozen of ps) of the temperature of the lattice through molecular vibrations and phonon population [28,29]. This lattice warming can also result in its thermal expansion. However, it should be noted that the high spin state population becomes thermally equilibrated with the lattice in a time of the order of 10 μs, which corresponds to the "thermal step" in Fig. 1, much slower than the thermalization of the lattice. Thus the difference of the time scale of the thermalizations of lattice and spin state plays an important role for the elastic step and the thermal step.

B. Models and discussion

1. The thermo-mechano-elastic model

In order to discuss both elastic and thermal steps in the framework of a unified model, we use here a modified mechanoelastic model, which was previously applied to simulate the elastic self-amplification alone. In this model, the molecules, represented as rigid spheres, are situated in open boundary lattices. The elastic interactions are simulated by springs linking a molecule to its closest neighbors. When a molecule changes its state, its volume varies, which results in an immediate elongation or a compression of its closest springs, determining first the motion of neighboring molecules and then the propagation of the initial perturbation towards all the lattice.

The elastic simulations of spin crossover materials imply two processes: the switch of spins and the change in molecular positions [30]. The spin change may be performed either by the way of Metropolis criterion or by an Arrhenius approach, which is used here, as faster and more appropriate to dynamic phenomena. Because we study local spring interactions

among molecules, the strain effect (elastic interaction) is automatically taken into account,

Therefore every spin change will influence both neighboring and, in a smaller extent, far-away molecules. In this way, a single elastic constant stands for both short-range and long-range interactions.

Most of the simulations in this paper have been performed for a 2D rectangular shape system composed of 13 824 molecules in a triangular configurational bonding. The Arrhenius molecular switching probabilities of the ith spin between the LS and HS states depend on the "temperature" T, on intrinsic material parameters (the HS-LS energy difference D, the degeneracy ratio g, the effective activation energy E_A) and on the effective elastic interactions between molecules, represented here by the way of the local pressure force p_i acting on molecule i, and are explicitly given by in the following equations:

$$\begin{aligned} P^i_{\mathrm{HS}\to\mathrm{LS}} &= \frac{1}{\tau}\exp\left(-\frac{E_A-\kappa p_i}{k_B T_i}\right),\\ P^i_{\mathrm{LS}\to\mathrm{HS}} &= \frac{1}{\tau}\exp\left(-\frac{D-k_B T_i \ln g}{k_B T_i}\right)\\ &\quad\times\exp\left(-\frac{E_A+\kappa p_i}{k_B T_i}\right), \end{aligned} \tag{1}$$

where τ is a constant scaling factor ensuring that the probabilities are below unity, and κ a scaling constant linking the local pressure with the activation energy. We have to strengthen that the local pressure force is the key parameter of the model, as it can dramatically change the steady state of the system. Using a Monte Carlo standard procedure, one decides if a molecule switches or not by comparing its transition probability with a random number $\eta \in (0, 1)$. One Monte Carlo electronic step (MCES) is completed when every molecule has been checked once. After every MCES, the new positions of molecules must be found either by the mechanical relaxation of the lattice considering small displacements on all axes, using a Nose-Hoover formalism [20] or, as used here, by computing the motion of molecules solving the following system of differential equations for all molecules:

$$\begin{aligned} m\frac{d^2x_i}{dt^2} &= F_{i,x}-\mu\frac{dx_i}{dt}\\ m\frac{d^2y_i}{dt^2} &= F_{i,y}-\mu\frac{dy_i}{dt}, \end{aligned} \tag{2}$$

where x_i and y_i are the Cartesian coordinates of the molecule i, m is the mass of the molecule, μ is a damping constant, preventing the system to enter into an uncontrolled oscillatory motion, and F_{xi}, F_{yi} are the components of the instantaneous force $\overrightarrow{F_i}$ acting on molecule i given by the sum of the forces from the neighboring springs.

The number of steps r to solve the system of coupled differential equations after every MCES is a key ingredient for the transient evolution of the system [26,31]. The value of r, tunes the different time scales of spin dynamics and lattice relaxation and is a measure for how fast the lattice relaxation is in comparison with individual molecular switching. A large r favours equilibrium distribution, specific for static phenomena, whereas a smaller r favours nonequilibrium distribution as in the case of fast phenomena subsequent to femtoseconds photoexcitation experiments [30].

The steady state of the system before photoexcitation is generated by computing at least 5000 MCES at the given temperature (i.e., at 145 K where most of the simulations have been performed to reach the steady state corresponding to a X_{HS} of around 0.06). The material parameters used in simulations, in line with standard experimental calorimetric data for spin crossover systems [32,33], were $D = 1100$ K, $g = 1096$, thus giving a thermal transition temperature $[D/(k_B \ln(g))]$ of around 157 K. The radius of HS molecules is considered to be 0.22 nm, and that of LS molecules 0.2 nm. The distance between centres of molecules is 1.04 nm for two molecules in HS state and 1 nm for two molecules in LS state. These values correspond to x-ray experimental measurements for typical spin crossover compounds [32,33]. The elastic constant of intermolecular springs is $7\,\mathrm{N}/m$, which generates a moderate cooperativity in the system [34]. As in previous works, κ is taken $1450 \times 10^{-14} J/N$ while $\tau = 1000\,\mathrm{s}^{-1}$ [11,13].

Photoirradiation randomly transforms more molecules to the HS state in addition to those in the steady state. The temperature of the photoexcited molecules is increased by $\Delta T = 100$ K. The simulation starts immediately after the first thermalization and deals with the second and third thermalization, as described in the introduction. The heat propagates through the sample following the Fourier's law of heat conduction:

$$\frac{dQ}{dt} = -k\nabla T \tag{3}$$

with k denoting the thermal conductivity. Using the continuous equation of the heat and the relation $Q = \rho c_p T$, the equation of the distribution of the temperature is written after a few transformations [35] as

$$\frac{dT}{dt} = \frac{k}{\rho c_p}\nabla^2 T = D_T \nabla^2 T, \tag{4}$$

where ρ is the mass density, c_p the specific heat at constant pressure and D_T denotes the thermal diffusion constant.

Equation (4) can be approximately transposed by a finite difference method [35,36], considering two kinds of heat transfer, i.e., the diffusion in the bulk of system and the heat transfer to the bath (external), to the following equation of lattice temperature diffusion:

$$\frac{dT^i_L}{dt} = -\alpha\left(T^i_L - \left\langle T^i_L\right\rangle\right) - \beta\left(T^i_L - T_B\right), \tag{5}$$

where T^i_L is the lattice temperature of the ith molecule, $\langle T^i_L\rangle$ is the average of lattice temperatures for all neighbors of the ith molecule, α is the diffusion coefficient, T_B is the external thermal bath temperature and β is the heat transfer coefficient to the bath. By the second term at the right-hand side, which is considered for only edge molecules, the lattice temperature approaches the bath temperature from the edges to the inner part.

The algorithm for simulations is then completed within the thermoelastic model with the computation of temperatures of every molecule considering Eq. (5), after every update of all the spin state MCES after photoexcitation. Typical

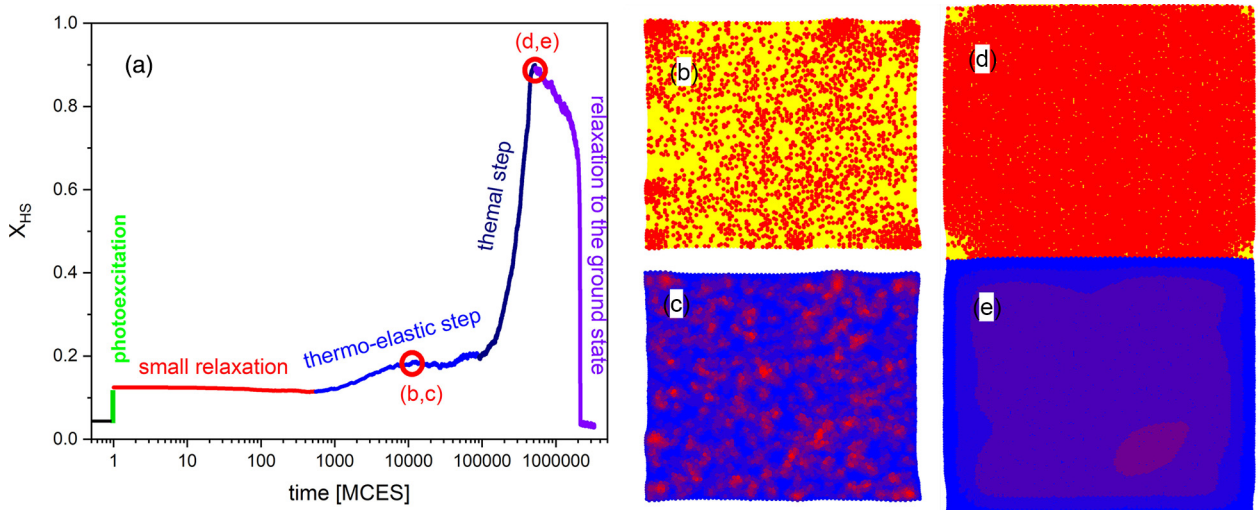

FIG. 2. Evolution of the system after ultrafast photoexcitation showing relaxation, thermoelastic step, thermal step and the final relaxation to the ground state. (a) Snapshots of the system at the maximum of the thermoelastic step [(b) and (c)] and at the maximum of the thermal step [(d) and (e)]. Spin states maps [(b) and (d)]: red circles: HS molecules, yellow circles: LS molecules; down: temperature map). Temperature maps [(c) and (e)] blue: low temperature, red: high temperature

results of simulations using Eq. (1) coupled with Eq. (5), where $T_L^i = T_i$ are presented in Fig. 2(a) for coefficients $\alpha = 0.0005\,\mathrm{MCES}^{-1}$, $\beta = 0.001\,\mathrm{MCES}^{-1}$, after 10% photoexcitation at 145 K. Both the thermoelastic and the thermal step were reproduced using these parameters and the distributions of temperature are marked in the figure with a color scale. Just after the photoexcitation, the newly switched HS molecules are subject to large local pressures, due to their increase in size, which determines the immediate compression of neighboring springs. These large pressures determine a small relaxation of the system, due the switching back of several HS molecules to the lower volume LS state experimentally reported [7,8]. The subsequent lattice relaxation leads to a decreasing of local pressure, which is a trigger for the thermoelastic step—the increase in number of HS molecules. Because the local pressure is smaller towards edges and corners due to geometric considerations (less neighbors), accumulations of HS molecules (small clusters) mostly appear in outer parts of the lattice [Fig. 2(b)]. Later on, the energy due the photoexcitation is distributed in the whole system and has the effect of the increase of the temperature of the whole sample above the critical temperature T_C and a large number of molecules switch to HS state [Figs. 2(d) and 2(e)]. However, this slow thermalization over the whole lattice is not compatible to the experimental fact that the energy is distributed very rapidly to the whole lattice uniformly as mentioned above. This problem will be resolved in the following. Finally, due to heat transfer to the external bath, the temperature in the system slowly decreases to the initial one and most of the molecules switch back to their ground LS state.

As we have discussed in the previous paragraph, all the macroscopic phenomena are successfully reproduced within the present model. However, in the introductory part, we have claimed that the thermalization of the lattice is very fast, and happens long time before the thermal step, as discussed even in early works concerning the photoinduced molecular switching [37]. Within this aspect, the results presented in Fig. 2(c) indicates a weakness of the present approach: we notice that at the maximum of the thermoelastic step, the distribution of the temperature in the lattice is very large; actually, the thermalization of the lattice is produced in the same time as the thermal step. In order to avoid this drawback, we propose in the following two alternatives of the current model corresponding to different thermalization processes of different subsystems. In previous works on ultrafast magnetism, the different thermalization timescales and energy transfert between electron, spin and lattice have been described through different temporal evolution of their respective temperatures. It was shown that they are equilibrated in the irradiated material after a very short time (about 5 ps) [38–41] the photoinduced out-of-equilibrium dynamics in Bismuth was discussed in terms of equilibration of electronic and lattice subsystems [42,43]. In the present work, we use an analogy to describe multiscale thermal equilibration.

2. The thermo-mechano-elastic model including a two thermalization sequence

The multiscale out-of-equilibrium dynamics induced by a femtosecond laser pulse in spin crossover materials and the subsequent thermalizations of the different degrees of freedom are different from what occurs in ultrafast magnetism or coherent phonons, for which the energy is deposited on delocalized electrons which thermalize rapidly as heated up by the laser pulse. Indeed, in the case of spin crossover materials, the energy is locally deposited on switched molecules that absorbed photons. We therefore consider different subsystems – the "hot" molecules locally photoswitched from low to high spin state due to optical excitation, the lattice heated up by energy transfert and expanding due to molecular swelling and the spin state of the molecules on the lattice, which equilibrate on a different timescales.

The difference between the equilibration times and the thermal step times suggests that the conversions driven by pressure and by temperature must be of different natures. While the local pressure excites the vibration modes implied in the volume change during LS-HS switching (spin states or breathing modes), the heat is transmitted from the lattice to all the vibration modes and, only in a subsequent process the spin state equilibrates. Indeed, this degree of freedom has longer equilibrations timescale and is therefore frozen on short timescales. Consequently, in order that the thermal transition takes place, an energy transfert is required from the hot lattice to the breathing modes, corresponding to the molecular reaction coordinate from LS to HS state, but the heated molecule needs enough time to explore the different molecular configurations and reach the maximum entropy HS state.

The difference between the timescales of the lattice thermalization and the macroscopic spin state equilibration with the hot lattice can be accounted for in the frame of our thermoelastic model by considering two temperatures: the "lattice temperature" (T_L) which corresponds to all lattice vibration modes and the "molecular spin state temperature" (T_S) to describe the thermal activation of the breathing vibration modes, which is directly connected to the LS-HS switching probabilities. We also denote as T_S^* the initial temperature of photoexcited molecules and T_B the temperature of the external thermal bath (cryostat, polymer, etc.) which corresponds to the initial (prior to photoexcitation) and final (after the relaxation of the thermal step) temperatures. The energy transfers and "temperatures" (we use quotes as the concept of temperature, necessary in the model, is different at the level of a single molecule) can be summarized as follows [see Fig. 3(a)].

(1) Ultrafast photoexcitation: the light transforms some of the LS molecules into hot photoexcited molecules with T_S^*.

(2) Photoexcited molecules release their energy towards neighboring lattice: first thermalization within $t_{\mathrm{ML}} \approx 10\,\mathrm{ps}$ [7]. After this stage the molecular spin state temperature of photoexcited molecules and the lattice temperature are equal: $T_S(t_{\mathrm{ML}}) = T_L(t_{\mathrm{ML}}) = T_B + \Delta T$, while for the other molecules $T_L(t_{\mathrm{ML}}) = T_B + \Delta T > T_S(t_{\mathrm{ML}})$, where ΔT is the molecular temperature jump. It depends on the number of switched molecules as $\Delta T = n_{\mathrm{photon}} \Delta E$, where n_{photon} is the density of photoexcited molecules and ΔE is the energy injected by a photon.

(3) Lattice towards spin state: the energy transfert from lattice to molecule is responsible for a slower spin state switching, which is responsible for slower thermal population of the HS state within $t_{SS} \approx 10\,\mu\mathrm{s}$. In this stage, the spin temperature becomes close to the lattice temperature, and the conversion from LS to HS at nonphotoexcited molecules takes place. After this step, the global thermalization of the subsystems is reached with equal temperatures [44].

(4) System towards bath: third thermalization within $t_B \approx 1\,\mu\mathrm{s}$–$1\,\mathrm{ms}$. In this step, the energy injected by photoirradiation is released to the bath. This step ensures that the "temperatures" of the ensemble reaches the temperature of the bath (this time varies as a function of system size, and the process takes place from the border to the inner places of the sample), so that the system recovers initial equilibrium state prior to photoexcitation.

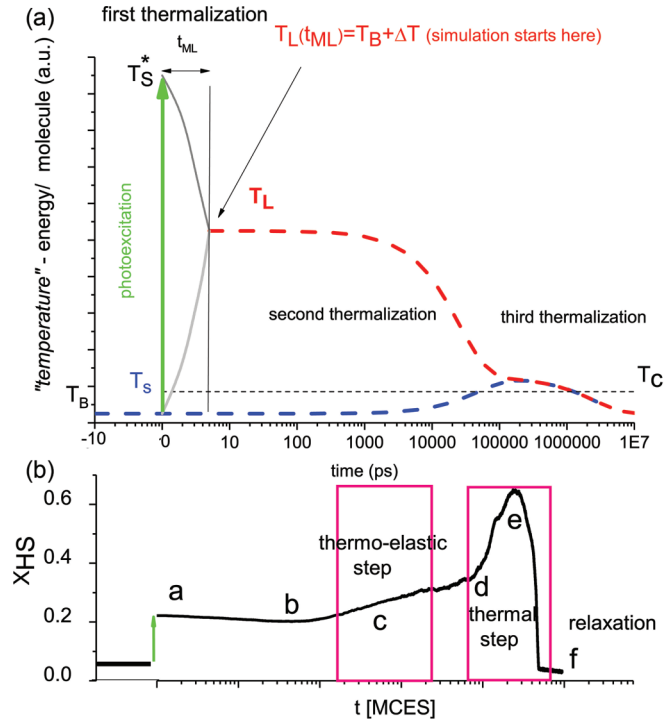

FIG. 3. (a) Schema for the behavior of the system after ultrafast photoexcitation: T_S-like, molecular (spin state) temperature, corresponds only to breathing modes; T_S^* is the temperature of converted molecules just after photoexcitation; T_L, lattice temperature, corresponds to all vibrational modes, T_C is the critical temperature. Before excitation, all subsystems have the same temperature, which is the temperature of the bath T_B. (b) Simulations using the mechanoelastic model for the 2D system and correspondence between the thermalizations and the elastic, thermal step and relaxation towards initial state.

To be in accord with these statements, we need to extend Eq. (5) to describe the equilibration of the spin state through the equilibration of its temperature. Thus we introduce a model in which Eq. (5) is phenomenologically coupled to the equation of temperature diffusion from the lattice towards the breathing (spin state) modes:

$$\frac{dT_S^i}{dt} = -\gamma\left(T_S^i - T_L^i\right), \tag{6}$$

where γ is the spin-lattice interaction constant.

Using this model with appropriate values for the thermal coefficients ($\alpha = 0.005\ \mathrm{MCS}^{-1}$, $\beta = 0.005\ \mathrm{MCS}^{-1}$, $\gamma = 510^{-5}\ \mathrm{MCS}^{-1}$), we have simulated the evolution of the system presented in Fig. 3(b). Let us analyze the evolution of the system. Only a small spin state relaxation can be observed just after photoexcitation (b mark in Fig. 3); due to the fact that most of the photoexcited molecules are found in a high-pressure environment, some of the HS molecules switch back to the smaller volume LS state. However, the increase of the temperature of the photoexcited molecule due to the laser pulse prevents the switching back of more molecules. The subsequent expansion of the volume of the whole lattice will decrease the pressure on all molecules in the system, therefore a large part of molecules, especially those on edge or corners,

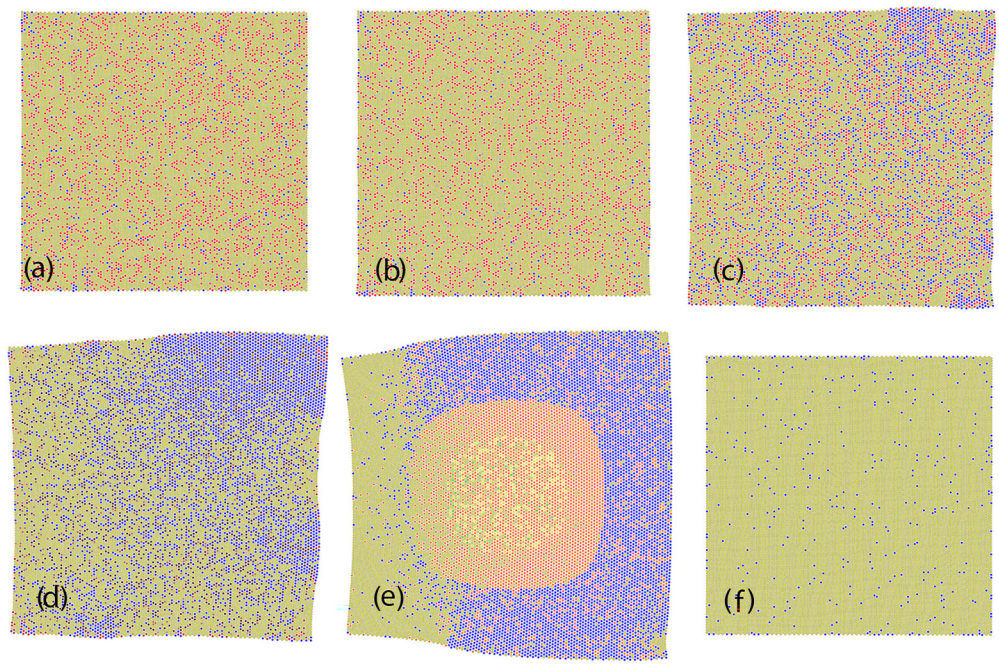

FIG. 4. Snapshots of a 2D system just after photoexcitation (a), during the small relaxation following the photoexcitation (b), at the maximum of the elastic step (c), at the beginning of the thermal step (d), at the maximum of the thermal step (e) and at the end of the final relaxation (f). Yellow: LS molecules, Blue, red, orange: HS molecules (from low to high temperatures, the scale is not the same for all figures). The letters correspond to those marked in Fig. 3, bottom.

are in low pressure environment, which helps HS molecules to keep their state and LS molecules to switch to HS state. To this stage, the molecular spin state temperature stays almost constant and the observed effects are of an elastic nature, except the role played by the initial increase of temperature, as explained above. Therefore this increase of the HS fraction has been denoted as elastic or thermoelastic step, because it is a thermally activated process, which is driven by elastic interactions [7,26]. The next process, observed after a longer time, relies on the global evolution of the temperature of the spin states in the system as resulting from Eqs. (5) and (6). Its significant variation can be detected much later, when it will determine the thermal switch of more LS molecules and producing the so-called thermal step. The final stage corresponds to the release of all the energy due to photoexcitation in the system towards the bath, and system comes back to the initial equilibrium state.

In Fig. 4, we present snapshots of the system, at different instants, before, during and after thermoelastic and thermal steps. The molecules are represented as circles with color code depending on their state and temperatures. In Fig. 4(a), we notice the presence of two kinds of HS molecules: blue spins with low temperature which are already populated at thermal equilibrium at the temperature of the bath T_B and red (or orange) spins with high temperature molecules which are switched by the laser. Figure 4(b) shows a configuration just after the small relaxation—the lattice volume stays unchanged at this step. There, the lattice volume stays unchanged at this stage, but due to the high pressure, many of high spins are converted to LS, and we see less density of high spins. After this high-pressure state, the lattice expands and some low spins converted to high spin state in the low pressure due to the expansion. Then, the reorganization of the lattice takes place, forming small HS molecules clusters at edges or corners, corresponding to the thermoelastic step as depicted in Fig. 4(c). After this point, the spin temperature increases and many low spins begin to be converted to the high spin state. At the beginning of the thermal step [Fig. 4(d)] the clusters formed during previous steps develop from corners and expand towards the center of the lattice. Figure 4(e) shows the configuration at the maximum of thermal step; at this stage we notice that the system starts to cool down from the edges to central part due to heat flow towards the environment. Finally, at the end of the relaxation, the temperature of all molecules came back to their initial temperatures, and only few molecules thermally populate the HS state at T_B, below T_C. In the system studied here, a local spin state is coupled to lattice and patterns of HS and LS molecules appear. Similarly, in a ferroelastic system [45], a coupling between strain and electrical local dipole moments leads to a pattern formation about polarity. Moiré-type patterns on the arrangements of HS and LS systems, have been recently observed on thin layers of spin crossover systems on substrates in appropriate elastic models [46].

The dependence of the thermal coefficients on the thermal step are presented in Fig. 5. As we explained before, because the temperature variation during the thermoelastic step is small, these coefficients do not influence the amplitude or the position of the thermoelastic step.

The role of the internal coefficient γ is explained in Fig. 5(a). When γ is large, the relaxation of T_S to T_L is fast, and thus the displacement of the thermal step appears at smaller values of the time. If the γ value is extremely large, the thermal step merges with the thermoelastic step. Reversely, a

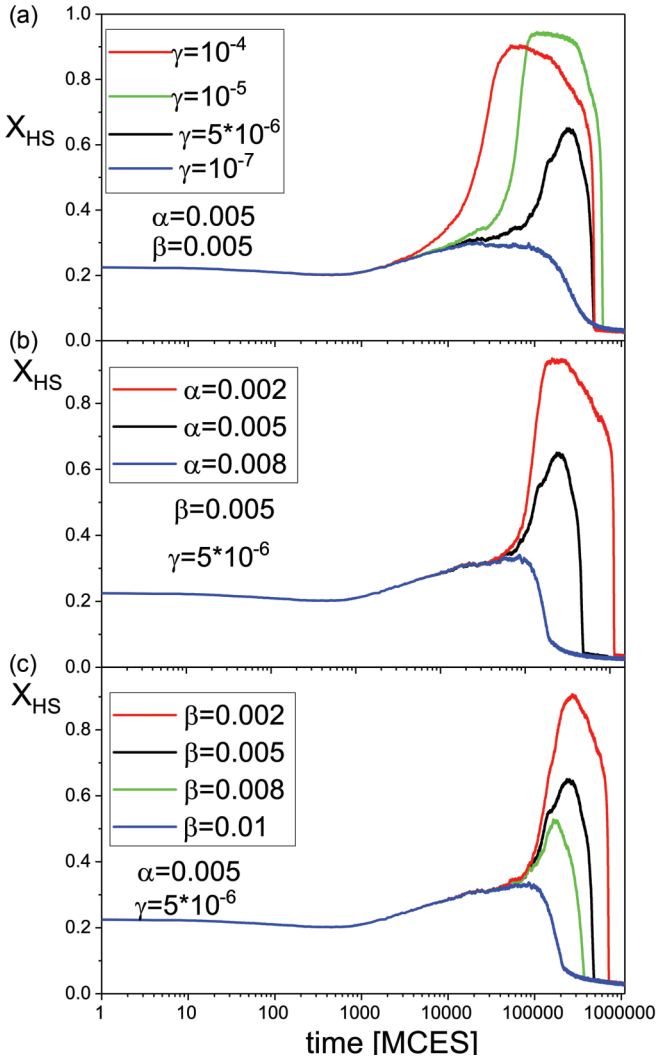

FIG. 5. Dependence of time evolution of X_{HS} on coefficients (a) γ, (b) α, and (c) β.

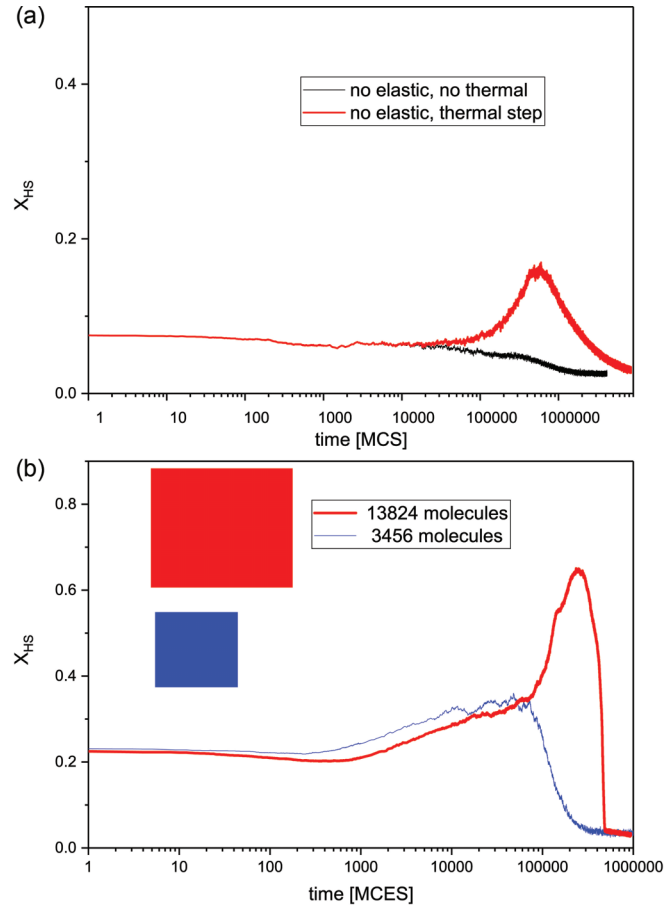

FIG. 6. (a) Dependence on the amount of photoexcitation. No elastic step and no thermal step take place (if the amount of energy transferred to the lattice is low). No elastic step, but thermal step takes place (for a higher amount of energy inside the lattice). (b) Size effects: the thermal step is observed only in the case of a larger system, for which the exchange with the thermal bath is slower.

small γ changes the molecular spin state temperature slower than the heat is lost towards the thermal bath, and, consequently, no thermal step is detected. The effect of thermal diffusion coefficients α and heat transfer coefficient β are analysed [Figs. 5(b) and 5(c)] and found to be quite similar. For larger values of α and β no thermal step is observed, which can be explained with data in Fig. 3(a): the thermal step occurs when the spin temperature becomes larger than the transition temperature T_C. For larger values of α and β, the decrease of molecular spin state temperature towards the bath is faster than its increase due to the energy received from the hot molecules via the lattice, so it does not reach the necessary T_C. Reversely, a larger thermal step is found for a slight change of the heat exchange with the bath, when the energy of hot molecules has the time to be transformed into internal energy of individual molecules.

Dependence on the amount of photoexcitation and on the size of the lattice are shown in Fig. 6. A smaller initial photoexcitation percentage (for example, obtained if using lower excitation density) does not allow the building up of the thermoelastic step. However, if the energy deposited initially on photoexcited molecules is high enough, then the temperature of the whole lattice increases enough to allow the presence of the thermal step, as experimentally shown in Fig. 1 for the smaller laser power. A trivial case of neither thermoelastic step nor thermal steps may be also obtained in experiments. The effect of a small size of the crystal which evacuate too fast the heat was also discussed in Ref. [12].

In Fig. 6(b), we present the size effects, simulating the behavior of two systems with different sizes (13 824 and 3456 molecules), while keeping all other parameters in the system the same. In a smaller sample the heat escape to exchange with the bath is faster, and thus, in small samples, the temperature will not surpass the critical temperature. This corresponds to experimental data shown in Fig. 1, where the thermal step is observed only in the case of crystals, and there is no thermal step in nanoparticles. In addition, we notice that in the case of the small sample the height of the elastic step has the same value as in the case of the large sample, but it shifts towards shorter times. This is due to the fact that in a smaller sample the elastic wave reaches sooner the borders of the sample. For the same reason, the relaxation after photoexcitation is less intense.

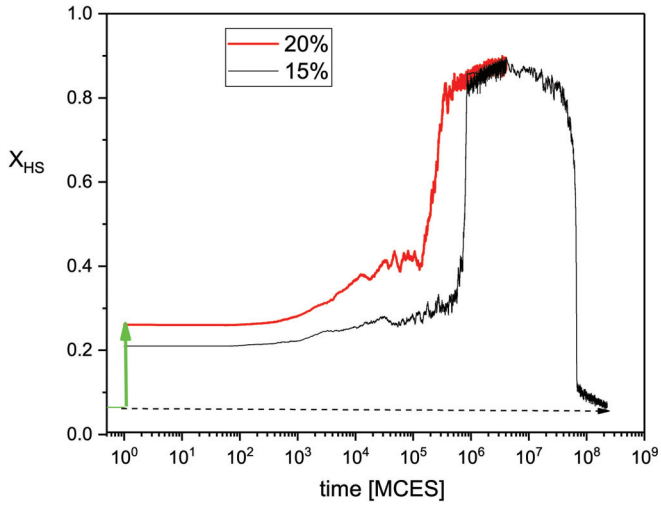

FIG. 7. Simulations using the mechanoelastic model for the 3D system for two initial photoexcitation rates.

3. 3D simulations of the two thermalization scales model

The 2D models can be considered to give a reasonable approximation for conceptual understanding of the phenomena, especially for layered spin crossover compounds with small interactions between the layers. However, several spin crossover systems present a three-dimensional structure, with the strength of interactions between planes on the same order as within planes and therefore it is important to extend the model towards 3D systems. Due to difficulties related to complexity of the system and the increased number of molecules, less studies have been devoted to modeling 3D systems except some works with open boundaries [47–49] or on surfaces [50–52]. In this section we use a rectangular cuboid system composed of 11 layers of molecules in a face-centred-cubic configuration. Each layer is composed of 1900 molecules in a triangular configuration; every bulk molecule is linked to its twelve closest neighboring molecules (six on the same plane, three below and three above) by springs; molecules on surface layers and those situated on the edge have less neighbors. The probabilities and the thermal diffusion equations are similar as for the 2D case; we have to note that in the 3D systems the molecules are allowed to move outside their initial planes to produce more favourable energetic conditions, leading to so-called buckling effects [47], which have been treated in previous papers for 3D systems of various shapes [48] or for monolayers of spin crossover molecules on substrates, leading to moiré patterns [46]. In Fig. 7, we present the whole curves obtained after 15% and 20% percentage photoexcitation, using the following transfer coefficient parameters $\alpha = 5 \times 10^{-7}$ MCES^{-1}, $\beta = 5 \times 10^{-7}$ MCES^{-1}, and $\gamma = 10^{-6}$ MCES^{-1}. As in the case of 2D systems we notice the well-defined presence of both the thermoelastic and thermal step. The amplitude of the thermoelastic step is larger

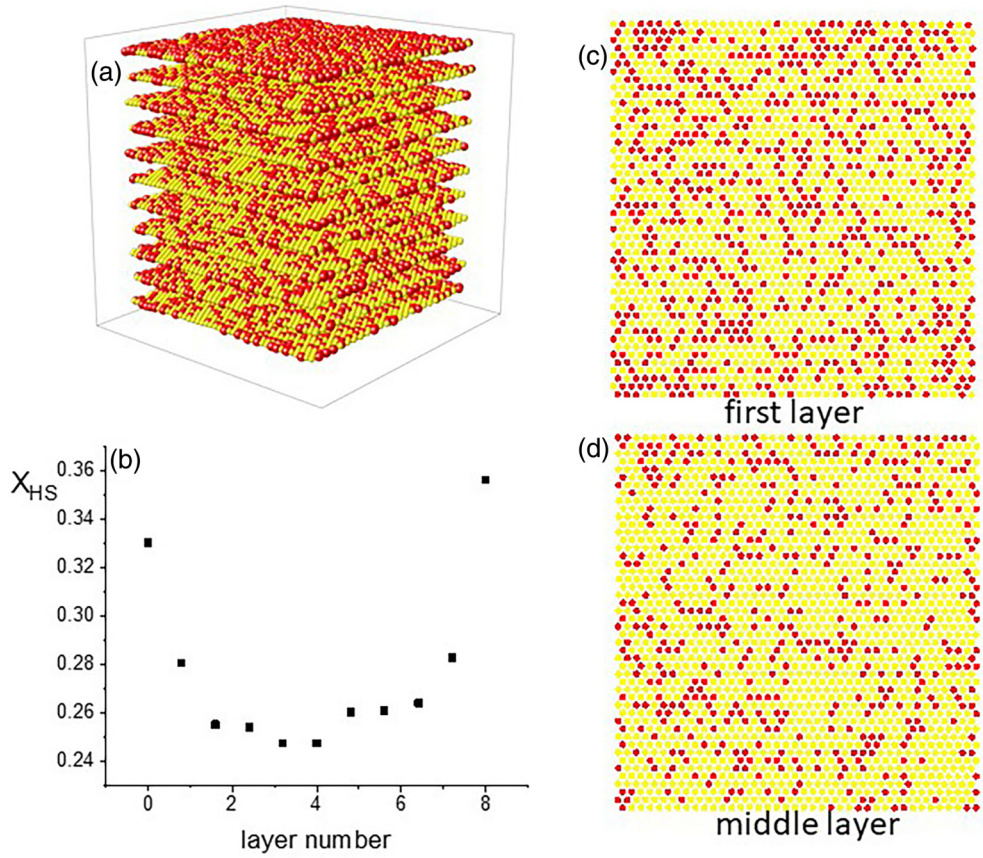

FIG. 8. A snapshot of 3D system at the maximum of the elastic step (a), snapshots of the first (c) and middle layer (d). The dependence of X_{HS} on the position of layers are shown in (b).

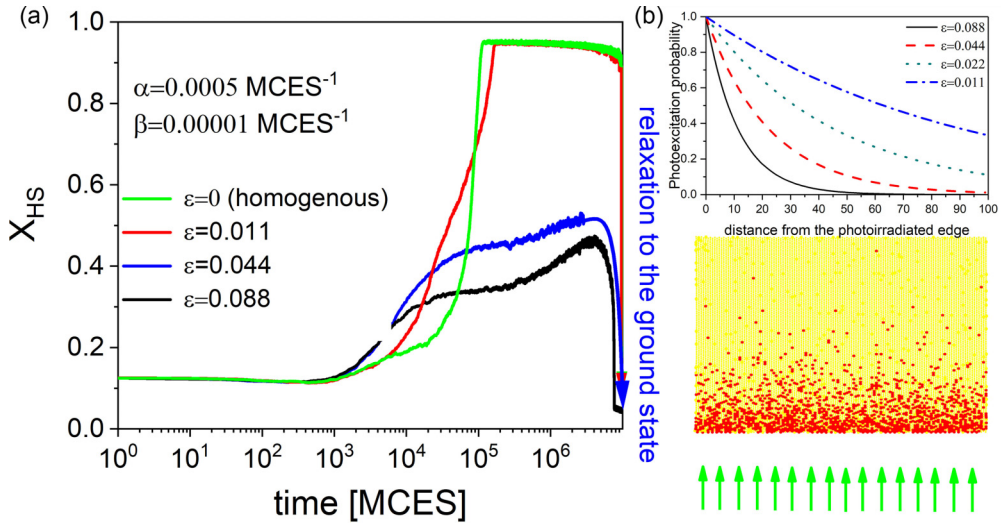

FIG. 9. (a) Evolution of the system after photoexcitation for different light absorptions (b) Decrease of the photoexcitation probabilities with x for different absorption coefficients ε. Snapshot of the system after photoexcitation for $\varepsilon = 0.088$.

in the case of higher initial photoexcitation, as previously observed in experiments [7] and simulations [10].

We refer now to the configuration of the system during the thermoelastic step. As specified above, in a 2D system a reorganization of the molecules in the system is observed at the maximum of the elastic step, consisting of the accumulation of HS molecules towards edges and corners. We analyze here the molecular configuration at the maximum of the elastic step for a 3D configuration. In Fig. 8(a), we present a snapshot of the whole system after 30000 MCS, while the snapshots of the first and middle layers are presented in Fig. 8(c) and respectively Fig. 8(d). At first sight, we notice a higher proportion of HS molecules in the first layer comparing to the middle layer. A quantitative analysis showing the X_{HS} for every layer is presented in Fig. 8(b) and confirms the initial observation: there are more HS molecules in the layers near the surface and their number decreases in the layers situated towards the center of the sample. Therefore we can conclude that in 3D systems the out-of-equilibrium molecular reorganization is similar to the one visible in 2D systems.

4. The case of inhomogenous photoexcitation

In this section, we refer to the simple thermo-mechano-elastic model, including only the lattice temperature, but we consider an inhomogenous photoexcitation, which can be expected in the case of sample with size of the order or larger than the light penetration depth. The photoexcitation probability can be written as $P = \exp(-\varepsilon x)$, where ε is the absorption coefficient and x is the distance of a molecule from the front of irradiation. The effect of the absorption coefficient on the distribution of the photoexcited molecules is depicted in Fig. 9(b). In the same figure, we present the evolution of the system keeping constant the heat transfer parameters and varying the absorption coefficient. We find that the homogenous case ($\varepsilon = 0$) gives a similar dependence

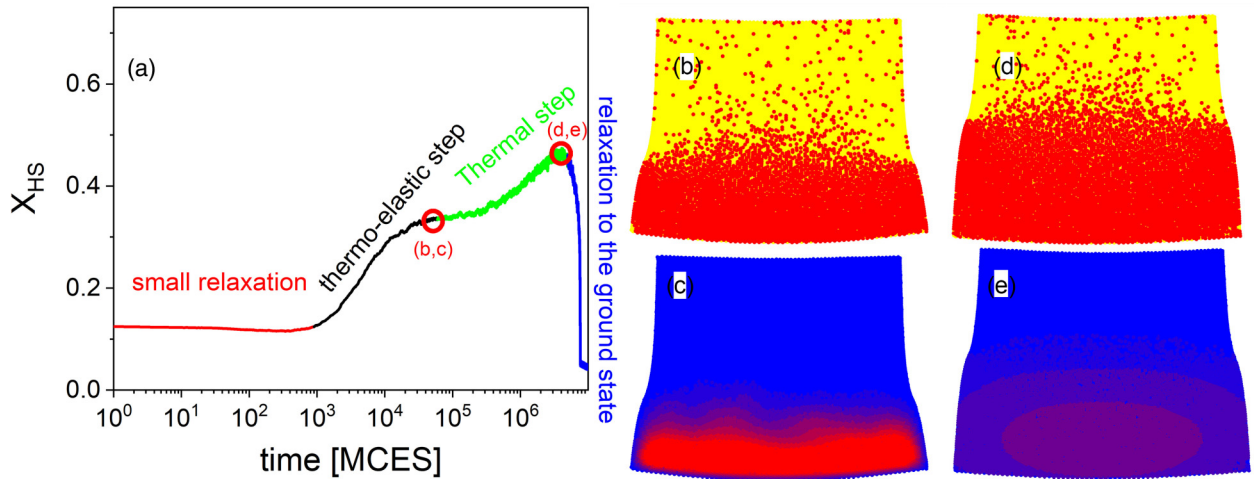

FIG. 10. (Left) Evolution of the X_{HS} after photoexcitation for $\varepsilon = 0.088$ (a). Snapshots of the system at the maximum of the thermoelastic step [(b) and (c)] and at the maximum of the thermal step [(d) and (e)], spin states map [(b) and (d)], and temperature map [(c) and (e)], using the same scale as in Fig. 2.

to that presented in Fig. 3. If the absorption is present ($\varepsilon \neq 0$), then a clearer disentangling between thermoelastic and elastic steps begins to be visible. Let us refer now to the case when $\varepsilon = 0.88$ which is presented in Fig. 10. In this situation the thermoelastic step and the thermal step are well separated, the amplitude of the elastic step is larger, while the amplitude of the thermal step is smaller than in Fig. 2, which correspond to experimental data. Actually, in some previous paper [7,10], the height of the simulated thermoelastic was smaller than the experimental one, so an inhomogenous photoexcitation could approach the simulated data to the experimental ones.

In Figs. 10(b)–10(e), we present snapshots of the system at the maximum of the thermoelastic step and during the thermal step. Unlike in the homogenous case, in the situation of an inhomogenous photoexcitation, the thermalization of the lattice is already realized at the maximum of the elastic step. The sample is then divided into two distinct parts, with different spin states and temperature. Later on, the temperature will propagate to the rest of the sample, causing the gradual transition of other LS molecules to HS state, which is the thermal step. The increase of the temperature will be however attenuated due to the bath and therefore, the amplitude of the thermal step will be smaller.

III. CONCLUSIONS

In this paper, in the framework of the 2D and 3D mechanoelastic models considering the heat transfer between thermal bath, lattice and molecular spin state subsystems, we have successfully reproduced both the thermoelastic and the thermal increase of HS population after femtosecond photoexcitation. The out-of-equilibrium dependences of HS fraction evolution $X(t)$ on the strength of irradiation and also on the size of system are systematically studied, i.e., the faster release of heat to the bath in the case of smaller systems is responsible for the absence of the thermal step which agrees with the observation in the case of nanoparticles in experiment. The present results, dealing with out-of-equilibrium thermalization and heat exchange between subsystems show that describing a complete out-of equilibrium dynamics from local molecular scale to macroscopic scale is complex. In addition to equilibration between subsystems, propagating (elastic waves) and diffusive (heat) phenomena must be taken into account. Equally, a most realistic study should consider the propagation of the heat by avalanches of more correlated regions, as it was theoretical stated in a review on the crackling noise in crystals, ferroelastic and porous materials [53]. Within this aspect, it would be interesting to determine a possible power law function describing the current multiscale phenomena. Similar approaches can be applied for other molecular systems with fast temperature variations or for spin crossover systems heated by plasmonic nanodevices [54]. It should be also noted that in the current method, the spin-transition is done by Monte Carlo sampling. Here we assume that the spin transition itself is much faster than the time scale of lattice motion. The spin transitions occur by contact with the thermal bath. Thus the comparison between the time scale of lattice motion and the that of contact with the bath is important. In principle, the ratio may result in different aspects of dynamics. This problem was studied by Nishino *et al.* [30], but so far, in our recent works, we used the present scheme to catch general aspects of dynamical phenomena. In the Monte Carlo simulations, the effect of degeneracies of HS and LS is treated in a thermodynamic approach, but not in a dynamical way. This must be investigated more carefully in the future. In principle, we may study the spin transition in the relation of lattice dynamics [55], but several fundamental problems remain to be studied. Thus, in particular for studies of dynamical properties, we should keep in mind these problems. But we still believe that the present work captures many important aspects of the system.

ACKNOWLEDGMENTS

The authors thank Prof. Hervé Cailleau for fruitful discussions during the manuscript preparation. S.M. acknowledges the hospitality of "JSR-UTokyo Collaboration Hub, CURIE". This work was supported by a grant of the Romanian Ministry of Research, Innovation and Digitization, CNCS/CCCDI-UEFISCDI, Project No. PN-III-P4-ID-PCE-2020-1946, within PNCDI III. The authors gratefully acknowledge Agence Nationale de la Recherche for financial support undergrant, ANR-19-CE30-0004 ELECTROPHONE, ANR-19-CE29-0018 MULTICROSS. E.C. thanks the University Rennes 1 and the Fondation Rennes1 for funding. The present work was supported by the Elements Strategy Initiative Center for Magnetic Materials (ESICMM) (Grant No. 12016013) funded by the Ministry of Education, Culture, Sports, Science and Technology (MEXT) of Japan, and was partially supported by Grants-in-Aid for Scientific Research C (Grant No. 18K03444 and No. 20K03809) from MEXT. This work was also supported by World Premier International Research Center Initiative (WPI), MEXT, Japan.

[1] P. Gütlich and A. Goodwin, *Spin Crossover in Transition Metal Compounds* (Springer, Heidelberg, 2004), Vols. I–III

[2] S. Zerdane, L. Wilbraham, M. Cammarata, O. Iasco, E. Riviere, M. L. Boillot, I. Ciofini, and E. Collet, Chem. Sci. **8**, 4978 (2017).

[3] A. Marino, P. Chakraborty, M. Servol, M. Lorenc, E. Collet, and A. Hauser, Angew. Chem. Int. Ed. **53**, 3863 (2014).

[4] S. Decurtins, P. Gütlich, C. P. Kohler, H. Spiering, and A. Hauser, Chem. Phys. Lett. **105**, 1 (1984).

[5] A. Hauser, Top. Curr. Chem. **234**, 155 (2004).

[6] E. Collet, L. Henry, L. Pineiro-Lopez, L. Toupet, and J. Real, CIC **6**, 61 (2016).

[7] R. Bertoni, M. Lorenc, H. Cailleau, A. Tissot, J. Laisney, M. Boillot, L. Stoleriu, A. Stancu, C. Enachescu, and E. Collet, Nat. Mater. **15**, 606 (2016).

[8] R. Bertoni, M. Lorenc, T. Graber, R. Henning, K. Moffat, J.-F. Létard, and E. Collet, Cryst. Eng. Comm. **18**, 7269 (2016).

[9] E. Collet, N. Moisan, C. Balde, R. Bertoni, E. Trzop, C. Laulhe, M. Lorenc, M. Servol, H. Cailleau, A. Tissot, M. L. Boillot, T. Graber, R. Henning, P. Coppens, and M. Buron-Le Cointe, Phys. Chem. Chem. Phys. **14**, 6192 (2012).

[10] C. Enachescu, L. Stoleriu, M. Nishino, S. Miyashita, A. Stancu, M. Lorenc, R. Bertoni, H. Cailleau, and E. Collet, Phys. Rev. B **95**, 224107 (2017).

[11] R. Bertoni, E. Collet, H. Cailleau, M. L. Boillot, A. Tissot, J. Laisney, C. Enachescu, and M. Lorenc, Phys. Chem. Chem. Phys. **21**, 6606 (2019).

[12] K. Ridier, A. C. Bas, V. Shalabaeva, W. Nicolazzi, L. Salmon, G. Molnar, A. Bousseksou, M. Lorenc, R. Bertoni, E. Collet, and H. Cailleau, Adv. Mater. **31**, 1901361 (2019).

[13] A. I. Popa, L. Stoleriu, and C. Enachescu, J. Appl. Phys. **129**, 131101 (2021).

[14] A. Slimani, K. Boukheddaden, and K. Yamashita, Phys. Rev. B **92**, 014111 (2015).

[15] W. Nicolazzi, S. Pillet, and C. Lecomte, Phys. Rev. B **78**, 174401 (2008).

[16] M. Nishino, K. Boukheddaden, Y. Konishi, and S. Miyashita, Phys. Rev. Lett. **98**, 247203 (2007).

[17] Y. Konishi, H. Tokoro, M. Nishino, and S. Miyashita, Phys. Rev. Lett. **100**, 067206 (2008).

[18] M. Nishino, Y. Singh, K. Boukheddaden, and S. Miyashita, J. Appl. Phys. **130**, 141102 (2021).

[19] C. Enachescu, L. Stoleriu, A. Stancu, and A. Hauser, Phys. Rev. Lett. **102**, 257204 (2009).

[20] C. Enachescu and W. Nicolazzi, Comptes Rendus Chimie **21**, 1179 (2018).

[21] R. Bertoni, M. Lorenc, A. Tissot, M. L. Boillot, and E. Collet, Coordination Chemistry Reviews **282-283**, 66 (2015).

[22] C. Enachescu, U. Oetliker, and A. Hauser, J. Phys. Chem. B **106**, 9540 (2002).

[23] S. Zerdane, E. Collet, X. Dong, S. F. Matar, H. F. Wang, C. Desplanches, G. Chastanet, M. Chollet, J. M. Glownia, H. T. Lemke, M. Lorenc, and M. Cammarata, Chem. Eur. J. **24**, 5064 (2018).

[24] M. Cammarata, R. Bertoni, M. Lorenc, H. Cailleau, S. Di Matteo, C. Mauriac, S. F. Matar, H. Lemke, M. Chollet, S. Ravy, C. Laulhé, J. F. Létard, and E. Collet, Phys. Rev. Lett. **113**, 227402 (2014).

[25] R. Field, L. C. Liu, W. Gawelda, C. Lu, and R. J. D. Miller, Chem. Eur. J. **22**, 5118 (2016).

[26] A. Volte, C. Mariette, R. Bertoni, M. Cammarata, X. Dong, E. Trzop, H. Cailleau, E. Collet, M. Levantino, M. Wulff, J. Kubicki, F.-L. Yang, M.-L. Boillot, B. Corraze, L. Stoleriu, C. Enachescu, and M. Lorenc, Commun. Phys. **5**, 168 (2022).

[27] M. von Allmen and A. Blatter, *Laser-Beam Interactions with Materials* (Springer, 1995).

[28] P. Ruello and V. E. Gusev, Ultrasonics **56**, 21 (2015).

[29] A. Marino, M. Cammarata, S. F. Matar, J. F. Letard, G. Chastanet, M. Chollet, J. M. Glownia, H. T. Lemke, and E. Collet, Struct. Dyn. **3**, 023605 (2016).

[30] M. Nishino, T. Nakada, C. Enachescu, K. Boukheddaden, and S. Miyashita, Phys. Rev. B **88**, 094303 (2013).

[31] M. Nishino, C. Enachescu, S. Miyashita, P. A. Rikvold, K. Boukheddaden, and F. Varret, Sci. Rep. **1**, 162 (2011).

[32] E. Konig, Structure and Bonding **76**, 51 (1991).

[33] P. Gütlich, A. Hauser, and H. Spiering, Angew. Chem. Int. Ed. Engl. **33**, 2024 (1994).

[34] C. Enachescu and A. Hauser, Phys. Chem. Chem. Phys. **18**, 20591 (2016).

[35] D. Sands, in *Heat Transfer - Engineering Applications*, edited by V. S. Vikhrenko (IntechOpen, 2011).

[36] V. A. Shneidman and M. C. Weinberg, J. Non-Cryst. Solids **194**, 145 (1996).

[37] H. Cailleau, M. Lorenc, L. Guerin, M. Servol, E. Collet, and M. Buron-Le Cointe, Acta Crystallogr A Found Crystallogr **66**, 189 (2010).

[38] E. Beaurepaire, J. C. Merle, A. Daunois, and J. Y. Bigot, Phys. Rev. Lett. **76**, 4250 (1996).

[39] B. Koopmans, G. Malinowski, F. D. Longa, D. Steiauf, M. Faehnle, T. Roth, M. Cinchetti, and M. Aeschlimann, Nat. Mater. **9**, 259 (2010).

[40] D. Zahn, F. Jakobs, Y. W. Windsor, H. Seiler, T. Vasileiadis, T. A. Butcher, Y. P. Qi, D. Engel, U. Atxitia, J. Vorberger, and R. Ernstorfer, Phys. Rev. Res. **3**, 023032 (2021).

[41] J. Kimling, J. Kimling, R. B. Wilson, B. Hebler, M. Albrecht, and D. G. Cahill, Phys. Rev. B **90**, 224408 (2014).

[42] T. Garl, E. G. Gamaly, D. Boschetto, A. V. Rode, B. Luther-Davies, and A. Rousse, Phys. Rev. B **78**, 134302 (2008).

[43] Y. Giret, A. Gellé, and B. Arnaud, Phys. Rev. Lett. **106**, 155503 (2011).

[44] M. Lorenc, C. Balde, W. Kaszub, A. Tissot, N. Moisan, M. Servol, M. Buron-Le Cointe, H. Cailleau, P. Chasle, P. Czarnecki, M. L. Boillot, and E. Collet, Phys. Rev. B **85**, 054302 (2012).

[45] H. Yokota, C. R. S. Haines, S. Matsumoto, N. Hasegawa, M. A. Carpenter, Y. Heo, A. Marin, E. K. H. Salje, and Y. Uesu, Phys. Rev. B **102**, 104117 (2020).

[46] A. Railean, M. Kelai, A. Bellec, V. Repain, M.-L. Boillot, T. Mallah, L. Stoleriu, and C. Enachescu, Phys. Rev. B **107**, 014304 (2023).

[47] K. Boukheddaden and A. Bailly-Reyre, Europhys. Lett. **103**, 26005 (2013).

[48] L. Stoleriu, M. Nishino, S. Miyashita, A. Stancu, A. Hauser, and C. Enachescu, Phys. Rev. B **96**, 064115 (2017).

[49] N. di Scala, N. E. I. Belmouri, M. A. P. Espejo, and K. Boukheddaden, Phys. Rev. B **106**, 014422 (2022).

[50] T. Delgado, C. Enachescu, A. Tissot, L. Guenee, A. Hauser, and C. Besnard, Phys. Chem. Chem. Phys. **20**, 12493 (2018).

[51] M. Kelai, V. Repain, A. Tauzin, W. B. Li, Y. Girard, J. Lagoute, S. Rousset, E. Otero, P. Sainctavit, M. A. Arrio, M. L. Boillot, T. Mallah, C. Enachescu, and A. Bellec, J. Phys. Chem. Lett. **12**, 6152 (2021).

[52] K. Affes, A. Slimani, Y. Singh, A. Maalej, and K. Boukheddaden, J. Phys.: Condens. Matter **32**, 255402 (2020).

[53] E. K. H. Salje and K. A. Dahmen, Ann. Rev. Condensed Matter. Phys. **5**, 233 (2014).

[54] Y. W. Hu, M. Picher, N. M. Tran, M. Palluel, L. Stoleriu, N. Daro, S. Mornet, C. Enachescu, E. Freysz, F. Banhart, and G. Chastanet, Adv. Mater. **33**, 2105586 (2021).

[55] M. Nishino, K. Boukheddaden, and S. Miyashita, Phys. Rev. B **79**, 012409 (2009).